Pergamon PII: S0038–092X(01)00070–6

Solar Energy Vol. 72, No. 1, pp. 1–11, 2002

Printed in Great Britain
0038-092X/02/$ - see front matter

www.elsevier.com/locate/solener

A HIGH-EFFICIENCY TRIPLE CYCLE FOR SOLAR POWER GENERATION

ABRAHAM KRIBUS[†,‡]
Environmental Sciences and Energy Research Department, Weizmann Institute of Science, Rehovot 76100, Israel

Received 28 November 2000; revised version accepted 17 May 2001

Communicated by LORIN VANT-HULL

Abstract—The last three decades have witnessed a trend in solar thermal electricity generation of increasing the concentration of sunlight, the operating temperature, and subsequently the efficiency of conversion from sunlight to electricity. The current state of the art concept is a solar-driven combined cycle, with sunlight concentration ratio of a few thousands, temperatures of about 1000–1300°C, and overall annual average conversion efficiency of about 20%. A possible next step in this trend is presented: a solar triple cycle, with a high-temperature MHD generator and two additional cycles in series. This triple cycle is powered by solar heat at temperatures around 2000°C and solar concentration of about 10,000. The overall peak conversion efficiency of the solar triple cycle is shown to be significantly higher than the solar combined cycle scheme. The sensitivity of this result to several system parameters and the technological feasibility of the solar triple cycle are also discussed. © 2002 Published by Elsevier Science Ltd.

1. INTRODUCTION

The last few decades have witnessed a clear trend in solar thermal electricity generation: increasing the concentration of sunlight, the operating temperature, and subsequently the efficiency of conversion from sunlight to electricity. The starting point was the solar pond, with no concentration, temperature around 100°C, and efficiency of around 1%. The next major advance was the parabolic trough, with concentration of less than 100, temperatures of 300–400°C, and annual average efficiency of around 10%. The next step is the solar tower system with steam generation, with concentration of a few hundred and temperatures of 500–700°C. The various versions of this concept all show annual efficiency of around 15% (Becker and Klimas, 1993). The recently proposed solar-driven combined cycle would provide temperature in the range of 1000–1300°C and concentration ratio of a few thousands. The annual average conversion efficiency of this system is predicted to be around 20% (Fraidenraich *et al*., 1991; Kribus *et al*., 1998b). This pursuit of ever-higher efficiency is economically motivated: sunlight is of course free, but collecting it is expensive. If we can generate more electricity from a given investment in solar collectors, then the solar electricity should become less expensive and more competitive.

In the conventional generation scene, efforts are also ongoing to increase the operating temperature of gas turbines, thereby improving their efficiency. Advanced gas turbines should soon operate around 1500°C, compared to a 1300°C limit only a few years ago. Such advanced gas turbines should provide heat-to-electricity conversion efficiency approaching 60% in a combined cycle mode (Facchini *et al*., 2000). A major step to significantly higher temperatures can be provided by a different technology: the magneto-hydro-dynamic (MHD) cycle. In this process, an ionized hot gas passes through a magnetic field. When this gaseous conductor cuts across the magnetic flux, current is generated in the direction perpendicular to the field and the flow. An MHD cycle can operate in the temperature range of 2000–2500°C, since the conversion to electricity is direct and there are no turbine blades or other sensitive objects in the flow path. Together with appropriate bottoming cycles, the MHD cycle should provide a very high conversion efficiency, possibly approaching 70% (Cicconradi *et al*., 1997; Kayukawa, 2000). In addition, an MHD cycle can use abundant fuel such as coal and does not require a high-grade clean gaseous fuel as gas turbines do. MHD technology is still in its infancy, but several development efforts and demonstration plants have been reported (Messerle, 1995).

[†]Tel.: 972-8-9343766; fax: 972-8-9344124; e-mail: nvi.kribus@weizmann.nc.il
[‡]Member of ISES.

A possible next step in the trend of increasing efficiency of solar thermal conversion is considered here: a solar triple cycle. This system includes a high-temperature MHD generator and two bottoming cycles. Can solar energy provide the very high temperature that is required for an MHD cycle? We note that the sun is an effective source at nearly 5500°C (Duffie and Beckman, 1991). Therefore, temperatures exceeding 2000°C should be feasible, given appropriate concentration of the incident sunlight. The theoretical limit on the concentration of sunlight is about 40,000. Current solar collector technology can provide a concentration of several thousands, using heliostat fields and secondary non-imaging concentrators (Karni *et al*., 1997; Kribus *et al*., 1998b). Increasing the concentration while minimizing optical losses is a challenging task, but with innovative optical solutions and improvement of solar collector technology, it should be possible to reach peak concentrations exceeding 10,000, possibly approaching 20,000 (Kribus, 1997). A simple calculation shows that given a concentration of 15,000 suns (a single 'sun' providing a nominal flux of 1 kW/m^2), a black absorber can convert incident radiation to heat at 2000°C with efficiency of 90%. Receiver temperature can go up to 2240°C if efficiency of 85% is acceptable. Solar heating at these temperatures is therefore feasible.

Using solar energy as the heat source for an MHD converter was first proposed three decades ago (Hildebrandt *et al*., 1972). It included a heliostat field with no secondary concentration, a hemispherical external receiver, and a simple MHD cycle with no bottoming. Since then, major advances have been achieved in our understanding of concentrating systems, solar receivers and MHD plants. The present paper incorporates these advances, as well as broadens the analysis to include a wide range of operating temperatures and the effects of other major system parameters.

The proposed solar triple cycle is composed of three conversion steps: a topping MHD cycle, an intermediate Brayton cycle gas turbine, and a bottoming steam Rankine cycle. The heat input is solar radiation delivered to the topping cycle. Using a relatively simple model, we optimize the efficiency of the entire plant for a range of operating temperatures, and compare the performance of the new solar triple cycle (STC) to the two-level solar combined cycle (SCC). The effect of the technological limits on pressure and temperature in several system components is discussed. The sensitivity of the results to model assumptions is also presented.

2. MODEL

2.1. Overview

The overall efficiency of a solar power plant is a product of three subsystem efficiencies: optics, receiver and power block

$$\eta_{\mathrm{Tot}} = \eta_{\mathrm{Opt}} \cdot \eta_{\mathrm{Rec}} \cdot \eta_{\mathrm{PB}}. \tag{1}$$

The optical efficiency depends on the type of concentrating system used; here we assume a solar tower and central receiver system, which is the only choice for large-scale high temperature solar processes. The optical efficiency accounts for losses due to imperfect reflections in the primary and secondary concentrators, and due to geometric losses such as shading and blocking in the heliostat field. The optical efficiency varies with time due to the motion of the sun, and here we consider the peak efficiency at the best time. The relation of this to annual average efficiency is discussed in Section 4. The solar receiver efficiency accounts for losses involved in the conversion of radiation to thermal power, such as intercept (spillage), convection, and thermal emission. At high receiver temperature ($T > 1000$°C) emission through the receiver's aperture is the predominating loss mechanism. Finally, the efficiency of conversion from heat to mechanical work and to electricity in the power block depends on the selection of the thermodynamic cycle. Detailed models for each of the three subsystems are presented in the following sections.

A system optimization process means finding the maximum total efficiency, by varying the main operational parameters: temperatures, pressures and solar concentration. Seeking separate optimal operating points for components or subsystems is not appropriate, since the main parameters tend to have contradictory effects on different components. For example, increasing the receiver temperature increases the power block efficiency, but reduces the receiver efficiency. The system then must be optimized as a whole rather than in separate sections.

2.2. Solar collector

The primary solar collector is a heliostat field with a central tower. The design of a heliostat field is an intricate process, including many details that are site-specific and application-specific (Winter *et al*., 1991). We use an idealized model of a field composed from very small

heliostats, packed as densely as possible, but without blocking losses (Riaz, 1976; Kribus *et al*., 1998a; Spirkl *et al*., 1998). The irradiation of the target by such a field is maximal. The maximum-density field model represents therefore an upper limit on collected power and incident receiver flux at design conditions. For simplicity, we assume that the field is circular, which is reasonable in locations near the equator. The field rim angle is made as large as possible to allow large-scale plants without resorting to unreasonably high towers. Solar concentration off-tower (SCOT) secondary concentration is selected (Kribus *et al*., 1998b), as shown in Fig. 1a. This option offers the highest concentration for large rim angle fields (Kribus *et al*., 1998a).

In a practical field design, the heliostat packing density will be less than the maximum possible, to avoid excessive shading losses in off-design conditions. This reduces the power collected at design point conditions, but increases the power collected at other times, and therefore can increase the annual average power. The variation of field density produces then the tradeoff of nominal concentration (proportional to collected power at design point) vs. annual average efficiency (proportional to the annual average collected power). However, the current study considers design point conditions only, since considering the annual average performance requires a much more complex model of the heliostat field. It is therefore not possible to include the variation in optical efficiency as part of the system optimization. The effect of reducing field density is therefore discussed below as a parametric change rather than as part of the optimization, and only in the context of peak efficiency.

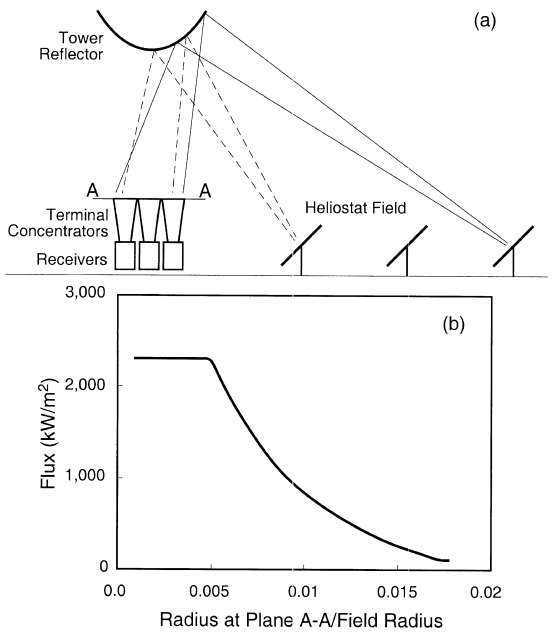

Fig. 1. (a) Schematic of a SCOT plant with a hyperboloid tower reflector and an array of terminal concentrators and receivers. (b) Irradiance flux distribution as a function of radial position at the plane of entrance to the terminal concentrator array. The peak flux at the center for a maximum density field is 2.3 MW/m^2. The flux entering the receiver located at the center of the array after terminal concentration is 11.1 MW/m^2.

We define a circular heliostat field where the rim angle of the field as seen from the aim point is 80°. For example, if the height of the aim point is 100 m, then the radius of the field is 567 m and the total power reaching the receiver aperture plane is 236 MW. Different power levels can be achieved with the same efficiency by scaling the optics as needed. The tower carries a hyperboloid reflector, suspended below the aim point, such that the radiation is reflected towards the secondary focus near ground level (Fig. 1). An array of terminal concentrators of CPC or CEC type (Kribus *et al*., 1998a) is placed at the target plane for the final concentration stage and connection to the receivers. For this design of the field and the secondary reflector, the terminal concentrators have an acceptance half-angle of 27°. We assume that the reflectivity of the heliostats, the tower reflector and the terminal concentrators is 0.9, 0.95 and 0.95, respectively. The direct normal insolation is 1000 W/m^2, and the sun is assumed at the zenith (i.e. design point conditions). The half-angle subtended by the sun is 7.5 mrad, which includes degradation due to the reflectors' surface errors. The geometric efficiency of the heliostat field due to the 'cosine effect' is 0.80 (Kribus *et al*., 1998a); there is no shading or blocking due to our definition of the ideally packed field and design point time. Adding the reflectivity losses due to the three stages of concentration, the overall optical efficiency is $\eta_{\mathrm{Opt}} = 0.65$.

In the optimization procedure presented below, we hold the solar field geometry fixed. When different power levels are needed, the entire field geometry is scaled, such that the efficiency remains fixed. The incident flux distribution at the receivers' apertures was computed by ray tracing for the idealized maximum-density field model (Kribus *et al*., 1998a), and is shown in Fig. 1b. For the maximum-density field under the assumptions stated above, the peak flux at the center of the distribution, after the terminal concentrators, is 11.1 MW/m^2. The collection radius on the

target plane is allowed to change. Reducing the collection radius reduces the intercept efficiency (increases the amount of spillage), but also increases the average flux incident on the receiver and hence the receiver efficiency. The collection radius is determined by the air inlet temperature into the receiver. The inlet temperature is not equal to the ambient temperature, since the air entering the receiver has undergone compression (see Section 2.4). If the incident flux at the rim is lower than the thermal emission flux corresponding to the inlet temperature, then the inlet region has a negative net contribution to the receiver. In this case, the collection radius can be decreased with a net gain in receiver power.

2.3. Solar receiver

Achieving high temperatures in a reasonably efficient solar receiver requires a non-isothermal, or partitioned, receiver (Ries *et al*., 1995; Kribus *et al*., 2000). Receiver losses depend strongly on the receiver temperature, and the main loss component in a high-temperature receiver is emission, which increases with the temperature to the fourth power. The partitioned receiver reduces these losses by dividing the receiver aperture into segments having different temperatures, and directing the fluid to be heated sequentially through these sections in the order of increasing irradiance flux and temperature. A large portion of the aperture is therefore at temperatures substantially lower than the receiver's maximum temperature, and the losses are significantly reduced relative to a thermally equilibrated or isothermal design.

We assume that the receiver is subject to emission losses only, and neglect convection and conduction losses. This is a reasonable assumption for a high temperature receiver, since the emission losses increase with the fourth power of the temperature, much faster than the other loss mechanisms. The receiver aperture is modeled as a black surface with a temperature that is low at the rim and gradually increases towards the center (Spirkl *et al*., 1997). The black receiver model serves as an upper bound on receiver performance, since real receivers are not black and are subject to an additional penalty in performance due to a temperature difference between the absorber and the fluid. The working fluid traverses the receiver array radially inward from the rim, and exits at the center.

The efficiency of a non-isothermal black receiver subject to the incident flux distribution $F(r)$ depends on the temperature distribution:

$$\eta_{\mathrm{Rec}} = 1 - \frac{\int_R^\infty F(r)\,2\pi r\,\mathrm{d}r + \sigma \int_0^R T_{\mathrm{Rec}}^4(r) 2\pi r\,\mathrm{d}r}{\int_0^\infty F(r) 2\pi r\,\mathrm{d}r}. \tag{2}$$

The first loss term is the spillage, and the second is thermal emission. The temperature distribution within the non-isothermal receiver, $T(r)$ in Eq. (2), is not known a-priori, and needs to be found from the flux distribution and the inlet temperature. We assume that the flow is from the rim radially inward, and that local heat transfer is perfect, such that the fluid and absorber temperatures are equal. The energy balance on a section of the receiver leads to a non-linear first-order differential equation for the temperature:

$$mC\,\mathrm{d}T_{\mathrm{Rec}} = -\left[F(r) - \sigma T_{\mathrm{Rec}}^4(r)\right] 2\pi r\,\mathrm{d}r. \tag{3}$$

Eq. (3) was solved numerically using fourth order Runge–Kutta integration, starting from the collection radius $r=R$ and up to the center $r=0$. The collection radius R is determined by the fluid inlet temperature: it is the largest radius where the term in square brackets in Eq. (3) is non-negative. This collection radius determines the spillage loss, as explained in the previous section. This loss is included in the receiver efficiency, as seen from the boundaries of the integral in Eq. (2).

2.4. Power block

We consider two options for the conversion from heat to electricity (Fig. 2): the traditional Brayton–Rankine combined cycle (CC), and a triple cycle (TC) with an MHD topping cycle, intermediate Brayton, and bottoming Rankine. There are several different ways for combining an MHD cycle with bottoming cycles, for example (Messerle, 1995; Cicconradi *et al*., 1997; Kayukawa, 2000). The scheme used in the present model was chosen for simplicity, and since the differences in performance between the different schemes are not great (Cicconradi *et al*., 1997). The steps of oxygen enrichment and preheating of the MHD inlet stream are eliminated, since they are not needed with solar heating.

Both the MHD and the gas turbine cycles considered here are open cycles with air as a working fluid. Closed cycles with other working fluids (e.g. helium) have also been proposed for either or both cycles. A closed cycle usually poses an additional technological challenge on the heat input side, since a very high temperature heat

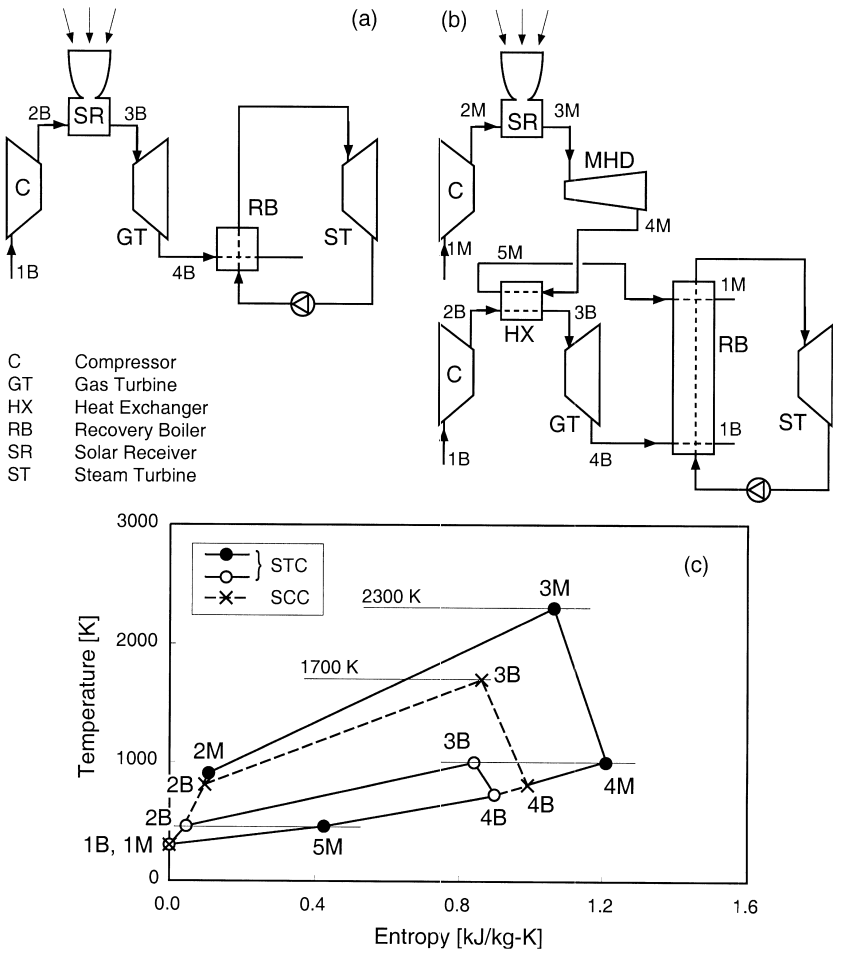

Fig. 2. Cycle schematics. (a) Solar combined cycle (SCC). (b) Solar triple cycle (STC). (c) Temperature–entropy diagrams for the topping cycle of the SCC with $T_{3B} = 1700$ K, and for the two upper cycles of the STC with $T_{3M} = 2300$ K.

exchanger is needed, replacing direct combustion within the gas in an open cycle. In a solarized cycle, such a heat exchanger is already provided: the solar receiver. Possibly, external heat supply from additional sources such as fossil fuel (hybridization) could be integrated into the receiver design. The issue of closed vs. open cycle, and the specific technology for heat input, were not addressed in the present analysis.

In the MHD cycle, the gas is compressed, heated and then expands in the MHD generator while doing work, similar to the Brayton cycle. The internal Joule heating has the same effect as frictional drag in a turbine, and the electrical output power is analogous to the shaft power of a turbine (Coombe, 1964). The MHD generator is therefore represented here as a Brayton cycle, and the details of the expansion process are represented in the effective turbine efficiency rather than explicitly treated (Messerle, 1995).

The Brayton cycle appears either as the topping level in the SCC system, or as both the topping and as the intermediate levels in the STC system. The specific work input to the compressor, and the specific work output from the turbine in the Brayton cycle, are:

$$w_{CB} = \frac{T_1}{\eta_{CB}} \left[\left(\frac{P_{2B}}{P_{1B}} \right)^{(\gamma-1)/\gamma} - 1 \right] \tag{4}$$

$$w_{TB} = T_{3B} \eta_{TB} \left[1 - \left(\frac{P_{4B}}{P_{3B}} \right)^{(\gamma-1)/\gamma} \right]. \tag{5}$$

The compression and expansion isentropic efficiencies η_{CB} and η_{TB} depend on the pressure ratio. They are derived using fixed values of the corresponding polytropic efficiencies, $\eta_{C,P}$ and $\eta_{T,P}$:

$$\eta_{CB} = \left(\frac{P_{2B}}{P_{1B}} - 1 \right) \left(\left(\frac{P_{2B}}{P_{1B}} \right)^{\eta_{C,P}} - 1 \right)^{-1} \tag{6}$$

$$\eta_{TB} = \left(1 - \left(\frac{P_{4B}}{P_{3B}} \right)^{\eta_{T,P}} \right) \left(1 - \frac{P_{4B}}{P_{3B}} \right)^{-1}. \tag{7}$$

We account for the pressure loss between the

compressor and turbine, representing the solar receiver (in a topping cycle) or the heat exchanger (in an intermediate cycle): $P_3/P_4 = \beta P_2/P_1$, with $\beta \le 1$. The low temperature T_1 is the ambient temperature (in an open cycle). The high temperature T_3 is the receiver exit temperature (topping cycle) or the heat exchanger exit (intermediate cycle). The other two temperatures are given by:

$$T_{2B} = T_{1B} + w_{CB}$$
$$T_{4B} = T_{3B} - w_{TB}. \quad (8)$$

The efficiency of a Brayton cycle (and of the MHD cycle modeled as a Brayton cycle), relative to the heat Q_B added between the compression and expansion steps, is:

$$\eta_{PB,B} = \frac{w_{TB} - w_{CB}}{Q_B} = \frac{w_{TB} - w_{CB}}{T_{3B} - T_{2B}}. \quad (9)$$

Heat for steam production is extracted from the exit of the topping cycle in the SCC, and from both the intermediate and topping (after the heat exchanger) cycles in the STC. The work output of the bottoming Rankine cycle is optimized as in Fraidenraich *et al.* (1991), leading to an optimal steam temperature of $T_S = (T_{4B}T_{1B})^{1/2}$. The steam specific work output is:

$$w_S = \eta_S(T_{4B} - T_S)(T_S - T_{1B})/T_S. \quad (10)$$

The conditions for the topping MHD cycle in the STC system are obtained by replacing the subscript B in Eqs. (4)–(9) with the subscript M, and replacing T_{4B} in Eq. (10) with T_{5M}.

The heat exchanger between the topping cycle and intermediate cycle in the STC is assumed to be matched: the heat capacity (mass flow rate times specific heat) of the two fluids is the same. The relation between the two cycles is then:

$$\varepsilon(mC)_{Min}(T_{4M} - T_{2B}) = (mC)_M(T_{4M} - T_{5M}) = (mC)_B(T_{3B} - T_{2B}). \quad (11)$$

The overall power block efficiency is the combined electricity output of all cycles, divided by the heat input. For the gas and steam turbines, an additional conversion from work to electricity is needed with an efficiency η_G. For the two-level SCC and the three-level STC, the overall power block efficiency η_{PB} is then:

$$\eta_{PB,CC} = \eta_G \frac{(w_{TB} - w_{CB}) + w_S}{Q_B} \quad (12)$$

$$\eta_{PB,TC} = \frac{(w_{TM} - w_{CM}) + \eta_G[(w_{TB} - w_{CB}) + w_S]}{Q_M}. \quad (13)$$

2.5. Technological limits

The model presented in the previous sections can be computed for a wide range of temperatures and pressures. However, practical systems have limited operation envelopes. We applied two limitations on the operation of the various components. One is a pressure limit of 30 bar on the Brayton cycles, representing the current operating limit of common gas turbines. We found that imposing this limit has a significant effect on the performance of a stand-alone Brayton cycle, but the effect on the SCC and STC performance was relatively small. The value of 30 bar that we chose is therefore not crucial; similar results would be obtained with different values. A variation on this assumption, limiting the topping MHD cycle to 10 bar while permitting the intermediate gas turbine to operate at up to 30 bar, is also discussed.

The second limitation is the temperature of the steam cycle. These cycles are usually limited to 300–350°C of saturated steam (in sub-critical systems) and about 600°C of the superheated steam. Our results showed that in the optimized systems, the steam temperature was always below 600 K, and therefore this technological limit had no effect on system performance.

2.6. Optimization procedure

We fixed the hot source temperature T_{3B} (or T_{3M} in the STC), and varied the compressor pressure ratio (both pressure ratios in the STC) to obtain the highest system efficiency according to Eq. (1). The mass flow rate through the receiver was constant, and we scaled the optics as needed until the desired receiver exit temperature was obtained. The value of the mass flow rate is only used as an intermediate value in Eq. (3), and does not affect the final result. The procedure was repeated for different values of the hot source temperature. The optimization used the Powell algorithm from Numerical Recipes (Press *et al.*, 1992). As mentioned in the previous section, the optimization was performed both without any limits, and with the technological limits (Brayton pressures, steam temperature) imposed on the optimization.

3. RESULTS

3.1. Double and triple cycles

Fig. 3a shows the total radiation-to-electricity conversion efficiency for the SCC and STC systems. Each point is separately optimized for the given hot source temperature T_3. The system

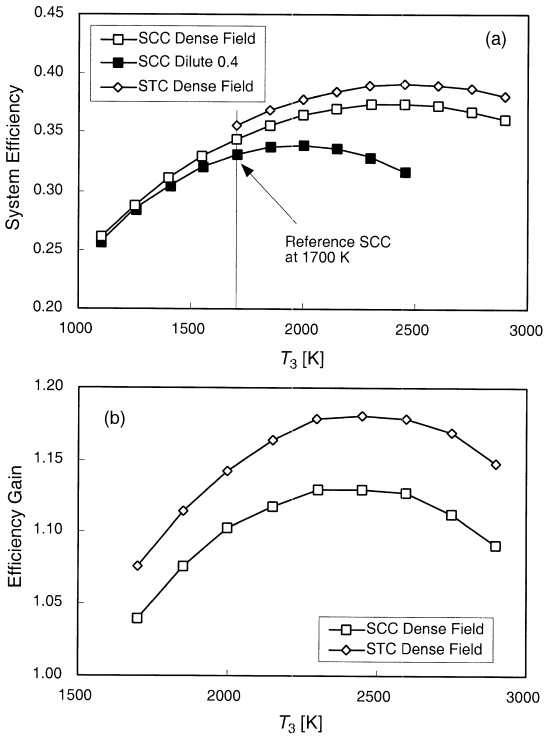

Fig. 3. (a) Efficiency of the optimized SCC with a maximum density heliostat field (most reflector area possible without blocking); the SCC with a field diluted to 40% of the maximum reflector area; and the STC with a maximum density field. The efficiency is shown as a function of receiver temperature. (b) Efficiency gain of the SCC and the STC relative to the reference SCC having a 40% diluted field and 1700 K receiver temperature.

parameters used are shown in Table 1. The efficiency shows a maximum for both systems since at high temperatures the receiver losses become significant and override the gain in power block efficiency. Two curves are shown for the SCC. The first is using the same ideal maximum-density heliostat field as used for the STC, corresponding to an area coverage ratio (heliostat area to ground area) of 0.36 and receiver inlet flux of 11.4 MW/m^2. The second result is for a diluted field, where the amount of heliostats is only 40% of the maximum density. This corresponds to a maximum incident flux on the receiver of 4.4 MW/m^2, and area coverage ratio of 0.14. This is a more reasonable design for the SCC, since the very high concentration provided by a dense field is not needed when the operating temperature is within the gas turbine range. Dilution of the field to a lower density lowers the flux distribution at the target plane, approximately by the dilution factor (if the dilution is uniformly applied over the entire field). The effects of field dilution on the STC are discussed in Section 3.4.

Table 1. System parameters used in the base case

Compression polytropic efficiency	$\eta_{C,P}$	0.90
Expansion polytropic efficiency	$\eta_{T,P}$	0.85
Pressure loss after compression	$1-\beta$	0.05
Steam cycle isentropic efficiency	η_S	0.90
Electrical generator efficiency	η_G	0.98
Heat exchanger effectiveness	ε	1.0
Optical efficiency	η_{Opt}	0.65

The difference between the SCC and the STC at the same temperature is small. However, the comparison of cycles at the same temperature is misleading, since the SCC is limited to the allowable temperatures of gas turbines, while the STC can operate at the much higher range of the MHD cycle. We define therefore the *efficiency gain*: the efficiency of a higher-temperature system divided by the efficiency of a reference SCC at 1700 K. The reference SCC temperature was chosen near the upper limit of current gas turbine technology. The diluted heliostat field case was chosen as more representative of a realistic solar plant. Fig. 3b shows that the STC provides a maximum gain of 1.18 in the range 2300–2600 K. Higher temperatures are not advantageous for the STC due to the increase in receiver losses. The SCC with the maximum-density field would have an efficiency gain of 1.13 relative to the reference plant, if it could sustain a temperature of 2300 K. Table 2 presents the main operation and performance parameters for the reference SCC, the optimal STC and several other cases that are discussed below.

The MHD exit temperatures shown in Table 2 are well below the ionization temperature, which is usually above 2000 K for common selections of

Table 2. Subsystem performance for the reference SCC, the base STC (defined in Table 1), and three other STC plant scenarios. These scenarios differ from the base case in a single parameter: pressure, expander efficiency, or heat exchanger effectiveness

Cycle	Ref. SCC	Base STC	STC $P<10$	STC $\eta_{T,P}=0.75$	STC $\varepsilon=0.9$
Receiver efficiency	0.93	0.93	0.95	0.94	0.93
Receiver exit temp. T_3 (K)	1700	2300	2300	2300	2300
MHD compression ratio	–	31.7	10.0	21.9	34.5
MHD exit temperature T_{4M} (K)	–	1008	1331	1200	985
Gas turbine compression ratio	22.2	3.8	6.3	5.2	4.3
Gas turbine exit temperature T_{4B} (K)	811	737	861	813	664
Heat exchanger exit temp. T_{5M} (K)	–	459	539	508	528
Total system efficiency η_{Tot}	0.331	0.390	0.378	0.369	0.383

working gas and seed. It would seem then that the gas would lose its conductivity somewhere along the MHD duct and the generation process would fail. However, due to the rapid expansion in the MHD duct, the bulk gas and the free electrons are not in equilibrium, and in effect, the electrons are 'frozen' in the ionized state. A common model of the MHD process defines an equivalent 'electron gas' that has a temperature that is distinct from the bulk gas temperature (Rosa, 1968). Therefore, an ionized state can be maintained even if the bulk temperature is too low for equilibrium ionization. A more detailed analysis of an MHD system should consider this effect to verify that ionization is maintained with a specific duct design.

3.2. Effects of pressure

Two pressure effects are considered here. One is the technology limitation on operating pressure. So far, we have assumed that both the MHD and the gas turbine can operate at any pressure. However, as the component's temperature increases, it becomes more difficult to contain high pressures due to a reduction in the strength of structural materials. Typical large gas turbines operate in the range of 10–30 bar, while MHD systems were considered at operating pressures such as 5–8 bar (Messerle, 1995; Cicconradi *et al*., 1997). We have repeated the optimization with a limit of 10 bar on the pressure of the MHD cycle, and 30 bar on the intermediate gas turbine. Fig. 4a shows that the efficiency gain is somewhat reduced under this pressure limit, and the maximum gain for the STC is 1.15.

The performance of a pressure-limited SCC with a maximum density field is also shown in Fig. 4a. The efficiency gain in this system is reduced when the pressure is limited to 30 bar, to efficiency gain of 1.08 at $T_3 = 2300$ K. This temperature cannot be achieved with a gas turbine, but one may consider a two-level combined cycle with an MHD and a single bottoming steam cycle. However, the pressure should then be limited to 10 bar, consistent with the discussion above for the MHD component of the STC. In this case, the performance drops sharply as seen in Fig. 4a, and the maximum gain is only 1.02 at 2300 K. The optimal pressure at this temperature is 42 bar, and the 10 bar limit strongly affects performance. The better option for the high-temperature MHD system is therefore the three-level STC which is less sensitive to pressure limitations.

The second aspect of the system pressure is the

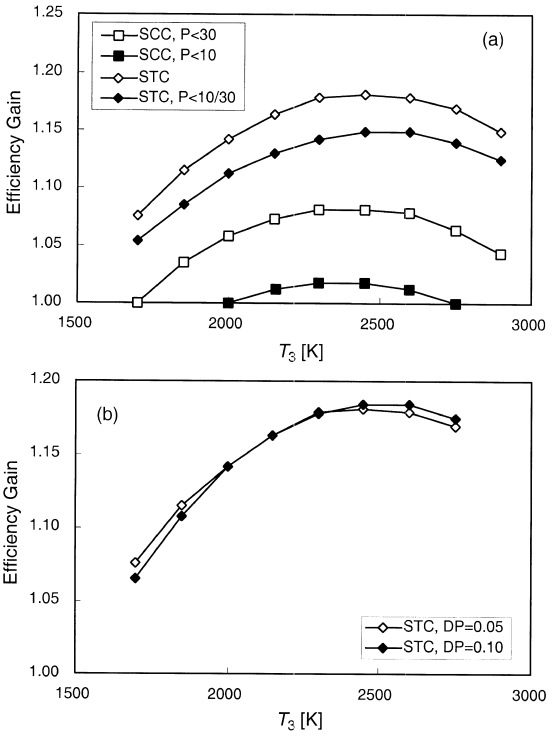

Fig. 4. Effects of system pressures. (a) Efficiency gain when MHD and gas turbine pressures are limited: the SCC is limited to 30 bar or 10 bar; the STC is limited to 10 bar in the MHD and 30 bar in the gas turbine. Pressure limitation has a strong effect on the SCC but a smaller effect on the STC. (b) Efficiency gain of the STC when the pressure drop between the compressor and the expander increases from 5 to 10%. The increase of pressure drop has a negligible effect on the STC efficiency gain.

pressure drop between the compressor exit and the expander inlet in both the MHD and the gas turbine cycles. In addition to the pressure drop found in any gas turbine due to the piping and the combustion chamber, here there are contributions due to the solar receiver (in the topping cycle) and the heat exchanger (in the intermediate cycle). Fig. 4b shows that the efficiency gain of the STC with 10% pressure drop ($\beta = 0.9$), relative to a corresponding SCC at the same conditions as the reference SCC, except that the pressure drop is also 10%. The gain is almost identical to the corresponding gain in the case of 5% pressure drop. The pressure drop has therefore practically no effect on the comparison of a high-temperature STC to a reference SCC having the same pressure drop.

3.3. MHD internal efficiency

In the previous sections, we have assumed certain values for the polytropic efficiency of the

components (compressors and expanders). The assumptions for the compressors and the gas turbine at intermediate temperature may be considered as reasonable, since these components are well known. However, the performance of the MHD expander cannot be predicted with the same level of certainty. The actual value of the polytropic efficiency in real devices depends on the MHD detailed design, which is outside the scope of the current work. Fig. 5 shows the sensitivity of the system efficiency gain to the assumption of MHD expander polytropic efficiency. For reduced polytropic efficiency of 0.8 and 0.75, the efficiency gain of the STC is reduced to 1.15 and 1.13, respectively. While this reduction is not negligible, the gain in performance relative to the reference SCC is still significant even for the lowest value of the MHD polytropic efficiency.

3.4. Solar field dilution

We have assumed above that the collector field for the STC has maximum density, producing the maximum possible flux at the receiver's inlet. In a real field, the packing density will be lower, to avoid excessive shading losses during off-design hours when the sun direction is far from the zenith. The desired value of field dilution factor should be found by an optimization of the annual performance, which is outside the scope of the current work. Fig. 6 shows the effect of field dilution on the efficiency gain at design point. The maximum efficiency gain is reduced to 1.15 and 1.12 for dilution of 0.8 and 0.6, respectively, compared to the original undiluted field providing a gain of 1.18. The efficiency gain is then sensitive to the field dilution and the resulting changes in flux level. However, there is a wide range for optimizing the heliostat field design for best annual performance, while still producing a significant design-point efficiency gain relative to the reference SCC.

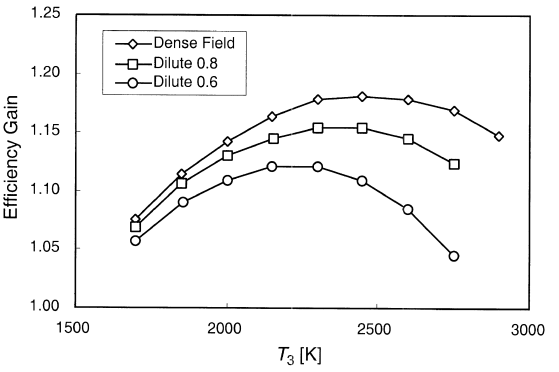

Fig. 6. Effect of heliostat field dilution on the STC efficiency gain. A maximum density field (reflective area is 36% of ground area) is compared to 0.8 field dilution (28.8% area ratio) and 0.6 dilution (21.6% area ratio).

3.5. Heat exchanger effectiveness

We have assumed that the heat exchanger between the topping MHD cycle and the intermediate gas turbine cycle is ideal, with effectiveness of unity. A more realistic value for the heat exchanger effectiveness should lower the performance of the intermediate and bottoming cycles. The sensitivity of the efficiency gain to the heat exchanger effectiveness is shown in Fig. 7. The results show an almost uniform decrease for all temperatures. The maximum efficiency gain is 1.16 and 1.14 for heat exchanger effectiveness of 0.9 and 0.8, respectively. System performance is therefore still much higher than the reference SCC even with a lower, more realistic heat exchanger effectiveness.

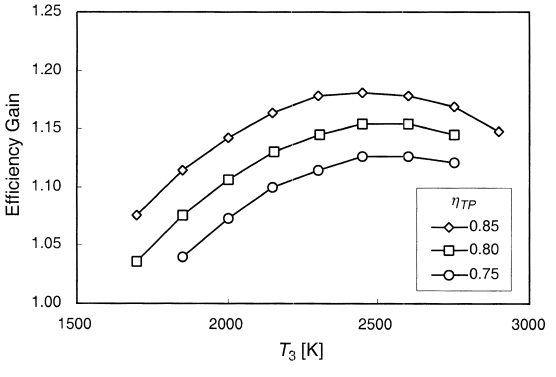

Fig. 5. Effect of reduction of the MHD expander polytropic efficiency on the STC efficiency gain. The base case of 0.85 expander efficiency is compared to 0.80 and 0.75.

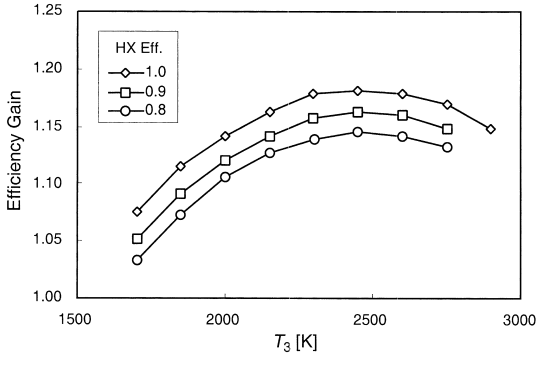

Fig. 7. Effect of the heat exchanger that couples the MHD outlet to the gas turbine inlet in the STC system. The efficiency gain with an ideal heat exchanger having effectiveness 1.0 is compared to effectiveness of 0.9 and 0.8.

4. DISCUSSION

We have shown that combining a high-performance solar collector field with an advanced high-temperature MHD plant and bottoming cycles has the potential for significantly higher peak (design-point) efficiency than a solar two-level combined cycle. The maximum advantage, or efficiency gain relative to a reference SCC, was obtained in most cases at receiver temperatures of about 2300 K. The efficiency gain depends on several system parameters, and varies between 1.1 and 1.18 for the cases presented here. It is also possible to operate at somewhat lower temperatures without a significant reduction in efficiency; however, the low temperature limit is also influenced by the MHD ionization conditions rather than determined by system efficiency alone.

Only design-point efficiency was considered in the current study. A quantity of higher interest, however, is the annual average efficiency. When comparing two alternative designs with differing field geometry or density, higher peak efficiency may or may not correspond to higher annual average efficiency. Computing the annual average efficiency requires a much more detailed model of the heliostat field, including description of the layout of individual heliostats; this is outside the scope of the current study. A solar plant optimized for best annual efficiency will also depend on additional specific parameters such as site, local insolation patterns, etc. A more detailed study is therefore needed before making any statements about the gain in annual efficiency.

The results reported in this work were derived using a simplified model of a solar plant, and it remains to be seen how close a real system may approach to the predictions of this model. Clearly, since both MHD and high-temperature solar technologies are still far from maturity, it is not possible to make very precise statements about their real performance. We have used the relative measure of the efficiency gain to circumvent this difficulty. It was assumed that the required solar and MHD components can reach the same level of technical maturity as the lower-temperature solar and combined cycle components have today. The relative measure provides then a reasonable comparison under a consistent set of assumptions. The sensitivity relative to major system parameters was also presented, and this should provide a reasonable sense of the range of variability for the efficiency gain results.

A major concern in all solar plants is operation when sunlight is insufficient or completely absent. Two possible solutions are hybridization and storage. Both of these are desirable in an STC plant. A hybrid STC would have a fuel combustion facility, using coal or another suitable fuel, operating at part load to provide supplementary heat whenever needed during daytime, and operating at full load when sunlight is not available. Such a hybrid plant would produce a significant advantage in CO_2 mitigation relative to conventional plants, both due to the solar contribution and due to the conversion of coal energy at very high efficiency compared to other coal technologies. However, a combustor that is downstream of a solar receiver would pose a significant technological challenge.

Thermal storage of excess solar energy during daytime may also be possible, using porous beds of ceramic storage media. Such high-temperature storage units are used today, for example in the glass industry, and could be adapted for use with a high-temperature power plant. The size of this storage could be much smaller than equivalent storage for lower-temperature solar plants, since the temperature difference between the inlet and outlet is much higher. Several major challenges would have to be addressed, such as minimizing the length and cost of high-temperature piping, and minimizing the pumping power associated with the additional flow channeled to the storage.

Some of the solar components of an STC need further development before they can be considered technically proven. Solar heliostat fields have usually been designed and operated at moderate concentration, around 1000. Increasing the concentration to the vicinity of 10,000 would require careful redesign and optimization, but there is no barrier or major technological breakthrough that is needed to achieve this. Thermal receivers operating around 2000 K have been constructed and tested, mostly for solar chemistry applications. However, these were lab-scale devices and it is not yet clear how a large-scale receiver with reasonable throughput and efficiency would be constructed. Most likely, a receiver at this temperature level will rely on direct absorption in a suspension of small particles within the working gas (Hunt and Brown, 1983). These particles may also play a useful role in the MHD process. However, particle receivers tested so far have not been able to heat gas to the expected high temperatures, and further work is needed in this direction. An additional area where further development is needed is the high-temperature heat exchanger, which is required between the MHD and gas turbine cycles.

The current work has shown significant potential for increased conversion efficiency. How-

ever, the 'bottom line' question in evaluation of any new technology is the eventual cost. It is not possible at this point to provide a meaningful estimate of the cost of electricity produced by the proposed STC. Two intermediate goals may be set, before attempting a full system cost analysis. The first is a more detailed system performance analysis, including optimization of a real heliostat field for very high concentration, and annual rather than design-point only performance. The second task is the development of high-temperature receiver technology in the range required by the MHD process. The demonstrated potential of improved efficiency supports the conclusion that such an ambitious long-range, forward-looking project could be a promising direction for the future of solar electricity production. This would also be consistent with the general trend in the solar as well as the conventional generation communities of increasing process temperature and efficiency.

NOMENCLATURE

C	specific heat (J/kg K)
F	flux (W/m^2)
m	mass flow rate (kg/s)
Q	specific heat addition (kW (kg/s)$^{-1}$ (kJ/kg K)$^{-1}$ = K)
r	radial coordinate on target plane (m)
P	pressure (bar)
R	collection radius (m)
T	temperature (K)
w	specific work (kW (kg/s)$^{-1}$ (kJ/kg K)$^{-1}$ = K)

Greek letters

β	pressure loss ratio
γ	ratio of specific heats, $\gamma = C_p/C_v$
ε	heat exchanger effectiveness
η	efficiency
σ	Stefan–Bolzmann constant

Superscripts and subscripts

B	Brayton cycle
C	compressor
G	generator
M	MHD cycle
Opt	optical
P	polytropic
PB	power block
Rec	receiver
S	steam Rankine cycle
T	turbine in Brayton cycle, or MHD section in MHD cycle
Tot	total

Acknowledgements—The author would like to thank J. Karni for useful discussions and exchange of ideas that led to this work.

REFERENCES

Becker M. and Klimas P. C. (1993). *Second Generation Central Receiver Technologies*, Verlag C.F. Müller, Karlsruhe.

Cicconradi S. P., Jannelli E. and Spazzafurno G. (1997) MHD plants: a comparison between two-level and three-level systems. *Energy Convers. Mgmt.* **38**, 525–531.

Coombe R. A. (1964). *Magnetohydrodynamic Generation*, Chapman and Hall, London.

Duffie J. A. and Beckman W. A. (1991). *Solar Engineering of Thermal Processes*, Wiley, New York.

Facchini B., Fiaschi D. and Manfrida G. (2000) Exergy analysis of combined cycles using latest generation gas turbines. *J. Eng. Gas Turbines Power* **122**, 233–238.

Fraidenraich N., Gordon J. M. and Tiba C. (1991) Optimization of gas-turbine combined cycles for solar energy and alternative power generation. *Solar Energy* **48**, 301–307.

Hildebrandt A. F., Haas G. M., Jenkins W. R. and Colaco J. P. (1972) Large-scale concentration and conversion of solar energy. *EOS* **53**, 684–692.

Hunt A. J. and Brown C. T. (1983) Solar test results of an advanced direct absorption high temperature gas receiver (SPHER). In 8th Solar World Congress, Vol. 2, pp. 959–963, Pergamon.

Karni J., Kribus A., Rubin R., Sagie D., Doron P. and Fiterman A. (1997) The DIAPR: a high-pressure, high-temperature solar receiver. *J. Solar Energy Eng.* **119**, 74–78.

Kayukawa N. (2000) Comparisons of MHD topping combined power generation systems. *Energy Convers. Mgmt.* **41**, 1953–1974.

Kribus A. (1997) Towards large-scale solar energy systems with peak concentration of 20,000 suns. In *Nonimaging Optics: Maximum Efficiency Light Transfer IV, Proc. SPIE3139*, pp. 178–185, San Diego.

Kribus A., Doron P., Karni J., Rubin R., Reuven R., Taragan E. and Duchan S. (2000) A multistage solar receiver: the route to high temperature. *Solar Energy* **67**, 3–11.

Kribus A., Krupkin V., Yogev A. and Spirkl W. (1998a) Performance limitations of heliostat fields. *J. Solar Energy Eng.* **120**, 240–246.

Kribus A., Zaibel Z., Segal A., Carey D. and Karni J. (1998b) A solar-driven combined cycle plant. *Solar Energy* **62**, 121–129.

Messerle H. K. (1995). *Magneto Hydrodynamic Electrical Power Generation*, Wiley, Chichester.

Press W. H., Teukolsky S. A., Vetterling W. T. and Flannery B. P. (1992). *Numerical Recipes in Fortran*, Cambridge University Press, New York.

Riaz M. R. (1976) A theory of concentrators of solar energy on a central receiver for electric power generation. *J. Eng. Power* **98**, 375–383.

Ries H., Kribus A. and Karni J. (1995) Non-isothermal receivers. *J. Solar Energy Eng.* **117**, 259–261.

Rosa R. J. (1968). *Magnetohydrodynamic Energy Conversion*, McGraw-Hill.

Spirkl W., Ries H. and Kribus A. (1997) Performance of surface and volumetric solar thermal absorbers. *J. Solar Energy Eng.* **119**, 152–155.

Spirkl W., Timinger A., Ries H., Kribus A. and Muschaweck J. (1998) Non-axisymmetric reflectors concentrating radiation from an asymmetric heliostat field onto a circular absorber. *Solar Energy* **63**, 23–30.

Winter C. J., Sizmann R. L. and Vant-Hull L. L. (1991). *Solar Power Plants*, Springer-Verlag, Berlin.